

# Electric earthquake precursors: from laboratory results to field observations

Filippos Vallianatos <sup>a,\*</sup>, Dimos Triantis <sup>b</sup>, Andreas Tzanis <sup>c</sup>, Cimon Anastasiadis <sup>b</sup>,  
Ilias Stavrakas <sup>b</sup>

<sup>a</sup> *Technological Educational Institute of Crete, Department of Natural Resources and Environment, 3 Romanou Street, Chania, Crete Island 73133, Greece*

<sup>b</sup> *Technological Educational Institution of Athens, Department of Electronics, Athens, Greece*

<sup>c</sup> *Department of Geophysics and Geothermy, University of Athens, Athens, Greece*

Received 6 July 2003; received in revised form 9 December 2003; accepted 16 December 2003

## Abstract

The generation of transient electric potential prior to rupture has been demonstrated in a number of laboratory experiments involving both dry and wet rock specimens. Several different electrification effects are responsible for these observations, however, piezoelectricity cannot explain why quartz-free rocks can also generate precursory phenomena and electrokinetic phenomena are normally very weak to produce macro- and megascopic scale effects. Electrification is observed in dry, non-piezoelectric rocks meaning that additional, solid state mechanisms should be responsible. Herein we focus on a promising effect that is ubiquitous during brittle rock failure: the motion of charged edge dislocations (MCD) during crack opening and propagation (microfracturing). We report a series of laboratory experiments on dry marble samples and discuss their possible relationship to field observations of purported electric earthquake precursors (EEP). The experiments confirm the generation of pressure-stimulated currents (PSC) as expected by the MCD model. The PSC was linearly related to the stress rate, so long as the stressed material deformed elastically. Deviation from linearity arose when the applied stress drove the specimen into the plastic deformation range; this effect has been attributed to the dependence of the PSC on the stress rate and, ultimately, to the inverse of the changing (decreasing) Young's modulus. The emitted current appears very intense and non-linear just prior to failure, where massive crack propagation implies massive MCD processes. Repeated cycles of deformation are associated with progressively weaker current emission, indicating the strong dependence of electrification on the residual damage. Overall, the results are consistent with, and render support to the concept of electrification by MCD/microfracturing. Other mechanisms cannot be excluded of course but are rather considered to accompany and supplement the drastic MCD process. The experiments cannot determine whether these process can scale up to earthquake-size volumes but they certainly do not contest the possibility. If so, the origin of the EEP would be massive crack formation and propagation, which in the case of earthquakes is expected to be a short-lived process at the terminal phase of the cycle. Observable macroscopic ULF field would be generated by the superposition of fields generated by multiple simultaneous individual cracks and would evolve in correspondence with the crack propagation process. It is possible to model the evolution of large crack ensembles and assess the expected time functions of transient EEP events: the result is a family of asymmetric-bell shaped time functions that may appear isolated or in groups. The model has been successfully applied to the analysis of real field observations.

© 2004 Elsevier Ltd. All rights reserved.

## 1. Introduction

Transient electric effects in the lithosphere, purportedly associated with seismogenetic processes, have been reported and studied for a long time. For instance, comprehensive reviews can be found in Park et al.

(1993); Johnston (1997) and Tzanis and Vallianatos (2001), while much additional information exists in the collections edited by Hayakawa and Fujinawa (1994), Hayakawa (1999) and Hayakawa and Molchanov (2002). The field observations instigated research into these effects. The generation of transient electric potential/current during the loading cycle prior to, and concurrently with rupture, has been demonstrated in a number of laboratory experiments involving both dry

\* Corresponding author.

E-mail address: [fvallian@chania.teiher.gr](mailto:fvallian@chania.teiher.gr) (F. Vallianatos).

and wet rock specimens. Electrification by microfracturing, i.e. the appearance of spontaneous charge production and transient electric and electromagnetic emission associated with the opening of microcracks, has been discussed by several authors, who also provided quantitative estimates of charge production and currents associated with microfracturing. For instance, Warwick et al. (1982), have measured current spikes from individual microcracks of the order of  $10^{-3}$  A, associated with crack opening times of the order of  $10^{-6}$  s, thus providing a net charge density of  $10^{-3}$  C/m<sup>2</sup>. A similar value of  $10^{-2}$  C/m<sup>2</sup> is reported by Ogawa et al. (1985), while Enomoto and Hashimoto (1990) measured a charge production of  $10^{-9}$  C for cracks with surface of the order  $10^{-6}$  m<sup>2</sup>, thus yielding a charge density of  $10^{-3}$  C/m<sup>2</sup>. Other experimenters, (e.g. Fiffolt et al., 1993; Chen et al., 1994; Enomoto et al., 1994; Hadjicontis and Mavromatou, 1994, 1996; Yoshida et al., 1994; Yoshida et al., 1997), observed simultaneous acoustic and E-EM signals, confirming that electrification effects arise during microfracturing. On an even larger scale, Tomizawa et al. (1994) observed direct ELF/VLF emission from underground explosions.

Although laboratory results are generally affirmative, there are two cardinal and inter-related problems hindering the compilation of viable, self-consistent theories of electrical earthquake precursor (EEP) generation and propagation. First, there is incomplete understanding of how laboratory results may scale up to the enormous, heterogeneous rock volumes involved in the preparation of large earthquakes. Second, the efficiency of the different electrification mechanisms is as yet unspecified and if more than one mechanisms are operative, their (constructive or destructive) interaction is poorly understood, as also is their individual contribution to the total effect. Hitherto theoretical attempts to address such questions were, usually, generically associated with some particular mechanism and produced different source geometries and propagation/decay laws (e.g. Gokhberg et al., 1985; Dobrovolsky et al., 1989; Varotsos et al., 1993; Slifkin, 1993; Bernard and Le Mouël, 1996; Vallianatos and Tzanis, 1999a; Tzanis and Vallianatos, 2002).

Electrokinetic effects (EKE), i.e. electrification due to the flow of water driven through permeable rock by crustal strain or gravity, have amply been demonstrated by laboratory experiments (e.g. Morgan et al., 1989, and references therein; Jouniaux and Pozzi, 1995a,b, 1997 and references therein). In fact, conditions suitable for EKE are very plausible, at least in the near-surface parts of seismogenic zones, and quite consistent with the wet models of the earthquake preparation process (for instance, the dilatancy-diffusion model of Scholz et al., 1973). In consequence, the EKE is a frequently quoted mechanism (e.g. Mizutani et al., 1976; Dobrovolsky et al., 1989; Bernard, 1992; Fenoglio et al., 1995; Ber-

nard and Le Mouël, 1996; other references therein). In a recent paper, Yoshida et al. (1998) suggested the EKE as the prime source of electric potential changes during microfracturing of saturated sandstone samples. Unfortunately, EK fields are weak and might be undetectable at long distances, partly because of natural limitations to the magnitude of the electrokinetic coupling coefficient contrasts and pressure differences necessary to drive strong currents. Laboratory measurements suggest that naturally occurring contrasts may be quite small, while conductive pore fluids may inhibit the coefficient and its increase as a function of permeability (Morgan et al., 1989; Jouniaux and Pozzi, 1995a). Considering also that the average stress drop of crustal earthquakes is 3 MPa, stress heterogeneities near active faults should seldom generate large-scale pressure differentials, sufficient to drive current with effects observable faraway from the source (e.g. see Tzanis et al., 2000). In the immediate vicinity of the fault zone, however, precursory signals may be caused by accelerating evolution of dilatancy, resulting in (forced) water flow into the dilatant region (e.g. experiments by Chen et al., 1994; Yoshida et al., 1998; Gensane et al., 1999; also theoretical models by Fenoglio et al., 1995; Patella et al., 1997). Still, it is rather difficult to obtain model potential differences higher than 30 mV above the source and almost impossible to get observable effects at distances of a few tens of km.

Piezoelectricity has been considered since the very early times of earthquake prediction research (e.g. Nitsan, 1977; Warwick et al., 1982; Yoshida et al., 1994, 1997). An objection to the feasibility of piezoelectric mechanisms is the possible self-cancellation of a macroscopic effect due to the expected random orientation of quartz crystals, unless a large proportion of them is aligned (e.g. Tuck et al., 1977). Nonetheless, experiments demonstrate the generation of macroscopic signals associated with microfracturing, (e.g. Enomoto et al., 1994; Yoshida et al., 1997 in simulated faults; Sasaoka et al., 1998), suggesting that piezoelectric signals may come from source regions of high stress rate, where the stress distribution takes the same value and geometry.

It is equally, if not more important, that E-EME was observed in completely quartz-free rocks (e.g. Fiffolt et al., 1993; Enomoto et al., 1994; Hadjicontis and Mavromatou, 1994, 1996; Freund and Borucki, 1999), while Vallianatos and Tzanis (1998, 1999a) showed that the stress sensitivity coefficient  $F = E/\dot{\sigma}$ , which determines the dependence of the transient electric field  $E$  on the applied stress rate, is comparable in both quartz-bearing and quartz-free rocks. Thus, additional electrification mechanisms have been considered, such as contact or separation electrification (Ogawa et al., 1985), the motion of charged dislocations (MCD) in the elastic (e.g. Slifkin, 1993; Hadjicontis and Mavromatou,

1994, 1996) and non-elastic domains (e.g. Ernst et al., 1993; Vallianatos and Tzanis, 1998, 1999a; Tzanis and Vallianatos, 2002), activation of positive hole type dormant charge carriers in quartz-free rocks (Freund and Borucki, 1999; Freund, 2000) and the electrification of trapped or flowing gases (Enomoto, 1996; Scudiero et al., 1998). Yet another mechanism that may result from large scale microfracturing involves current excitation due to the forced motion of conductive earth material in the geomagnetic field, by crack-emitted acoustic waves (Surkov, 1999).

What makes the MCD mechanism particularly attractive is the fact that it always occurs in association with brittle failure, since stress concentration and crack opening take place when, after some critical stress threshold, edge dislocations multiply, migrate and pile up against an obstacle. Dislocations may occur in different mechanical ‘flavours’ which would move in opposite directions under stress. Thus, although the dislocation density may be as high as  $10^{14} \text{ m}^{-2}$  for heavily deformed materials and both flavours carry comparable charges, any net electric polarization of one sign must result from the net excess of charged dislocations with a particular mechanical flavour. Such an excess can easily be the result of previous cycles of non-elastic deformation followed by healing. In the thermodynamic conditions of the schizosphere this process will result in an elongated electric dipole, oriented in the slip plane and perpendicular to the moving dislocation lines. Because the opening and propagation of cracks results in non-elastic deformation, the transient electric variation should be related to the non-stationary accumulation of deformation in the neighbourhood of the moving dislocations. It should also be expected that when ionic crystals and rocks undergo such drastic changes, more than one electrification mechanisms may be operative. It appears reasonable to suggest that moving dislocations, acting as stress concentrators, may guide and focus additional effects.

Charge production and current generation during crack opening is a short-lived effect. For dry rock conditions—resistivities  $\rho$  of the order  $10^6$ – $10^4$ —and common dielectric permittivities  $\epsilon_d$ , any charge and electromagnetic fluctuations with source dimension  $l \approx 10^{-4}$ – $10^{-1}$  m (typical cracks) will disappear after a time  $t_c \approx \epsilon_d \rho \approx 10^{-5}$ – $10^{-7}$  s (if no external sources are applied). This is comparable to the duration of crack opening ( $10^{-4}$ – $10^{-7}$  s). Charge production inside the crack is quickly destroyed by redistribution of the displacement currents and the current appears only while the crack propagates (for details see Tzanis and Vallianatos, 2002). If any long-lasting such signal is to be observed, it will have to be generated by the superposition of the signals from all the simultaneously propagating cracks and will evolve in time just like crack propagation. Accordingly, the electric field measured at

a point on the surface of the Earth located at distance  $r$  from the source and at time  $t_j$ , may be qualitatively expressed as

$$E(\mathbf{r}, t_j) \approx c_s \sum_{i=1}^{\dot{n}(t_j)} [\rho_i (J_{\text{MCD}} + J_{\text{O}})_i G(\mathbf{r}, \mathbf{r}_i) \left[ u(t_j) - u\left(t_j \frac{l_i}{v_i}\right) \right]] \quad (1)$$

where  $\dot{n}(t_j)$  is the number of active cracks at time  $t_j$ ,  $c_s$  is a sensitivity coefficient at the location of the receiver  $r$  and  $G(\mathbf{r}, \mathbf{r}_i)$  describes the propagation and attenuation of the dipole field generated by MCD ( $J_{\text{MCD}}$ ) and other ( $J_{\text{O}}$ ) effects due to a crack opening at point  $\mathbf{r}_i$ ;  $u(t_j)$  is the Heaviside step function;  $l_i$ , the crack propagation length and  $v_i$ , the opening velocity, so that the right-hand factor in the sum allows the  $i$ th crack to contribute only while it is opening. A determinative factor in this model is the magnitude of the function  $\dot{n}(t_j)$ , which must be large enough to form a macroscopic field. The dependence on resistivity is also a cardinal factor. As pointed out by Tzanis and Vallianatos (2001, 2002) resistivities of the order of  $100 \text{ } \Omega \text{ m}$  will cause charge redistribution to occur at nanosecond scale time constants, which is orders of magnitude faster than crack opening times and does not allow for a macroscopic field to build up, unless the number of cracks increases by a forbiddingly excessive factor. The result is consistent with the majority of laboratory experiments observing precursory electric signals in dry (i.e. resistive) rock samples and indicates that strong precursory fields due to solid state mechanisms are anticipated from resistive rock blocks. More work is needed in order to observe how wet rocks behave during microfracturing and only a few such experiments exist (Chen et al., 1994; Yoshida et al., 1998). We also note that due to charge generation a companion magnetic field is also expected and has been subject to intensive research (see the review of Tzanis and Vallianatos, 2001, and references therein). Further theoretical and experimental analysis of the magnetic component is given in Tzanis et al. (2000); Vallianatos and Tzanis (1999b, 2003) and references therein.

To summarize, the MCD/microfracturing electrification mechanism should be observable in non-piezoelectric rocks and should heavily depend on the mechanical conditions of the deforming material (damage accumulation, stress and strain rates) and its electrical properties. Given the right conditions, it could give rise to a macroscopic electric field by the superposition of the fields emitted by many simultaneously propagating cracks. These properties are testable in the laboratory and inspired the series of experiments reported herein. Because several generic theories of transient EEP production during the microfracturing of crustal rocks have been contrived and proposed (e.g. Molchanov and Hayakawa, 1998; Tzanis et al., 2000; Tzanis and Vallianatos, 2002),

ultimate objective of the experiments was to investigate whether the development of such models is worth pursuing, or should be abandoned for contradicting the almost unequivocal eventualities of carefully designed experiments. A positive outcome would at least imply that it is not unrealistic to extrapolate the effect to the scale of seismogenic volumes in order to explain some classes of purported EEP observations.

The rock samples were subjected to uniaxial compression at both variable and constant stress rates; measurements were made at all stages of the deformation process (elastic, non-elastic–plastic regions and up to failure. As prelude, we note that the emitted current ( $I$ ) depends on the stress rate ( $d\sigma/dt$ ) and inversely on the decreasing Young's modulus, in consistency with the MCD model.

## 2. The MCD electrification mechanism: an overview

The MCD model has been qualitatively described by Slifkin (1993) and further developed by Vallianatos and Tzanis (1998, 1999a) and Tzanis and Vallianatos (2002); only essential information will be given here. In a crystalline structure, dislocations may form by the excess or absence of a half-plane of atoms. The edge of this half-plane comprises a dislocation line, around which the physical fields related with it are concentrated. In an ionic structure there will be an excess or absence of a line of ions along the dislocation line, with consequence that the dislocation be charged. In thermal equilibrium, dislocation lines are surrounded by the Debye–Hueckel charge cloud and will be electrically neutral (Whitworth, 1975). In dynamic processes when dislocations move faster than the Debye–Hueckel cloud can follow, neutrality can no longer be maintained. Let  $A^+$  be the density of edge dislocations with the mechanical flavour required to accommodate uniaxial compression (or tension) and  $A^-$  the density of dislocation of the opposite type. The motion of charged dislocations produces a transverse polarization:

$$P = (A^+ - A^-) \cdot q_l \cdot \frac{\delta x}{\sqrt{2}} = \delta A \cdot q_l \cdot \frac{\delta x}{\sqrt{2}} \quad (2)$$

where  $q_l$  is the charge per unit length on the dislocation (of the order  $10^{-11}$  Cb/m). If screw dislocations are ignored, the plastic contribution to the strain, when these dislocations of Burger's vector  $\mathbf{b}$  move through a distance  $\delta\chi$ , is:

$$\varepsilon = (A^+ - A^-) \cdot \mathbf{b} \cdot \frac{\delta x}{2} \quad (3)$$

The rate of change in polarization is by definition equivalent to the electric current density. On using Eqs. (2) and (3) one can easily show that

$$J = \frac{\partial P}{\partial t} \Rightarrow J = \frac{\sqrt{2}}{\beta} \cdot \frac{q_l}{\mathbf{b}} \cdot \frac{d\varepsilon}{dt} \quad (4)$$

where  $\beta = (A^+ + A^-)/(A^+ - A^-)$ . Eq. (4) shows that the observed transient electric variation is related to the non-stationary accumulation of deformation. Notably,  $\beta$  usually assumes values between 1 and 1.5 in alkali halides (Whitworth, 1975). Assuming the highest value for rocks, i.e. lower excess dislocation density, and  $\partial\varepsilon/\partial t \approx 10^{-4} \text{ s}^{-1}$ , approximately equal to co-seismic deformation rates, we obtain  $J \approx \times 10^{-6} \text{ A/m}^2$  which is comparable to the values quoted from the experiments.

The purpose of the experiments was to investigate whether a pressure stimulated current (PSC), i.e. one produced by uniaxial compression of a rock sample, would behave as predicted by the MCD model. According to Eq. (4), the PSC is expected to be proportional to the strain rate  $\frac{d\varepsilon}{dt}$ . When the samples deforms elastically,

$$\sigma = Y_0 \cdot \varepsilon \quad (5)$$

where  $Y_0$  is the Young's modulus of the undamaged material and is constant in the elastic range. Consequently, it should be  $J \propto \frac{d\sigma}{dt}$ . Moreover, if  $\frac{d\sigma}{dt}$  is constant no transient PSC effect should be observed. When the stress exceeds the elastic limit, microcracks (damage) begin to form; further increase of the stress causes the microcracks to multiply and propagate and the material to deform non-elastically. In this case, the strain  $\varepsilon$  is greater than that expected by Eq. (5). Accordingly, the PSC amplitude is expected to increase when the stress rate (e.g. Turcotte et al., 2003),

$$\sigma = Y_{\text{eff}} \cdot \varepsilon \quad (6)$$

where  $Y_{\text{eff}}$  is the effective Young's modulus, which is no longer constant. With increasing stress and damage, the Young's modulus gets progressively smaller. Accordingly, the PSC amplitude is expected to decrease when the stress rate  $\frac{d\sigma}{dt}$  remains constant.

## 3. Laboratory results

In our experiments PSC were detected in Dionysos marbles collected from Mt. Penteli, Attica. The Dionysos marble, which has been typically used since the ancient times for the construction of artefacts and monuments, is mainly composed of calcite (98%) and other minerals depending on the variety of the marble, such as muscovite, sericite and chlorite (Kleftakis et al., 2000). Its content in quartz is very low, about 0.2%. Its density is  $2.7 \text{ g/cm}^3$  and its porosity is approximately 0.4%. Calcite crystals are polygonic, sometimes exhibiting twinning and mainly of equal size and their texture may be characterized as quasi-homoblastic. The rock is white with a few thin parallel ash-green colored veins

containing silver-shaded areas due to the existence of chlorite and muscovite. Matrix rocks were intentionally selected to be single-grained.

The experimental apparatus and technique have been duly described in previous work (Stavrakas et al., 2003) and only essential information will be given here. The experiment has been conducted in a Faraday shield to prevent electric noise from affecting the recorded signals. The noise-protected system comprised a uniaxial hydraulic load machine (Enerpac-RC106) that applied compressional stress to the sample, which was placed on a stainless steel base. The marble sample was placed between two thin Teflon plates, in the direction of stress, in order to provide electrical isolation. The values of the externally applied compressional stress were recorded using a manometer. A pair of electrodes was attached to the marble sample, using conductive paste. It has to be noted that the electrodes were attached in a direction perpendicular to the axis of the applied stress. The measuring system consisted of a sensitive programmable electrometer (Keithley 617) capable of resolving currents as low as 0.1 fA, and as high as 20 mA in 11 ranges.

Fig. 1 is a typical example of PSC (curve a) recorded during a stress jerk (curve b) in the elastic deformation range. Curve (c) shows the corresponding stress rate which, evidently, is proportional to the PSC amplitude. The proportionality between PSC can be expressed with the relationship

$$\gamma = \frac{I_{\max}}{(\frac{d\sigma}{dt})_{\max}} \quad (7)$$

where  $I_{\max}$  is the peak PSC value and  $(\frac{d\sigma}{dt})_{\max}$  is the corresponding peak stress rate.

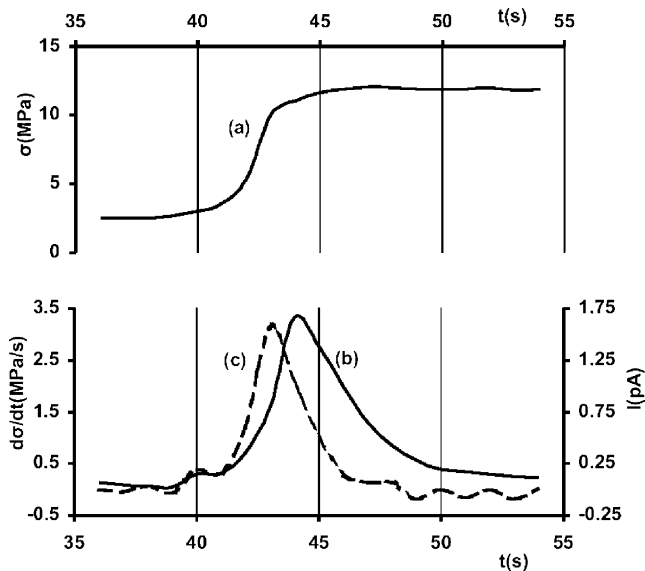


Fig. 1. Time recordings of: single variation of stress (curve a), the emitted PSC (curve b), the corresponding stress rate (curve c).

A large number of measurements of such peak PSC and stress rate pairs in both the elastic and the non-elastic deformation ranges, allows the experimental determination of  $\gamma$  and its variation as a function of the applied stress applied stress by using Eq. (7). Fig. 2 demonstrates the dependence of  $\gamma$  on the normalized stress  $\sigma/\sigma_{\max}$ , where  $\sigma_{\max}$  is the maximum stress sustained by the sample(s) and  $\sigma$  is the average stress during the jerk and is practically equal to the instantaneous stress at the time when the maximum stress rate  $(\frac{d\sigma}{dt})_{\max}$  is exerted. It is apparent that when the applied stress is less than  $0.6\sigma_{\max}$ , the value of  $\gamma$  remains practically constant. Consequently, for so long as  $\sigma/\sigma_{\max} < 0.6$ , the material behaves elastically and the Young's modulus remains constant. This becomes evident in the normalized stress–strain diagram of Fig. 3.

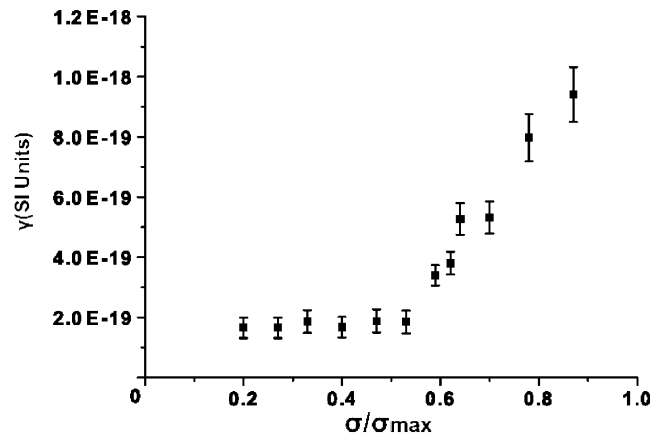


Fig. 2. Scaling factor  $\gamma$  with respect to the normalized stress.

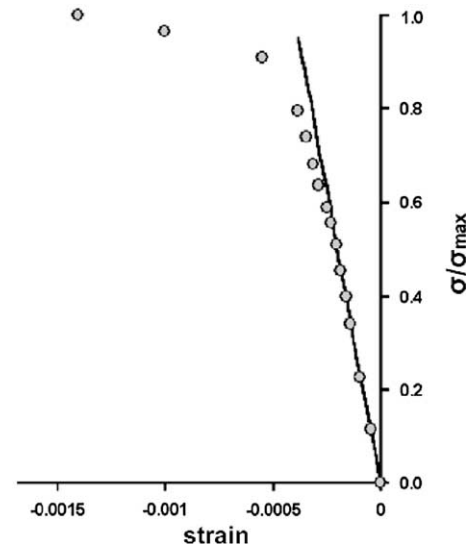


Fig. 3. Normalized experimental stress–strain diagram of Dionysos marble sample.

When  $\sigma = 0.6\sigma_{\max}$  the material gradually enters the plastic deformation range where the Young's modulus is continuously decreasing with increasing stress. Thus, combining Eqs. (4) and (6) it is easy to see that

$$J \propto \frac{1}{Y_{\text{eff}}} \cdot \frac{d\sigma}{dt} \quad (8)$$

and from Eqs. (7) and (8) it is evident that

$$\gamma \propto \frac{1}{Y_{\text{eff}}}$$

consistent with the experimental results.

From a microphysics point of view we note that in the plastic deformation range, structural changes are introduced into the samples depending on the stress state. According to Hallbauer et al. (1973), when the sample is stressed uniaxially in the early plastic stage, tensile microcracks begin to form. These are the dominant form of all heterogeneities that determine the process of failure (Lei et al., 2000): eventually, the increasing number of tensile microcracks tensile cracks at the lateral edges of shear cracks will reach a minimum critical distance with respect to each other and will begin to fuse; the array will be broken through by meso- and macro-scale cracks parallel to the shear plane, forming a shear process zone as the first stage in forming a rupture.

The PSC emission was also studied for samples subjected to a constant stress rate, beginning at zero stress and ending up to failure. The linear increase of stress with respect to time is depicted in Fig. 4 (curve a) and the rate was  $d\sigma/dt \approx 0.4$  MPa/s on a normalized stress axis. Fig. 4 (curve b) also shows the corresponding variation of the emitted PSC. It is evident that PSC only appears when stress is high enough for the material to enter the plastic range. At approximately  $0.8\sigma_{\max}$  a PSC peak was observed. At values greater than  $0.8\sigma_{\max}$  the PSC reversed polarity and developed into a negative spike-like extremum, which in absolute values was much larger than the maximum measured positive PSC value; such a behaviour is observed systematically just before

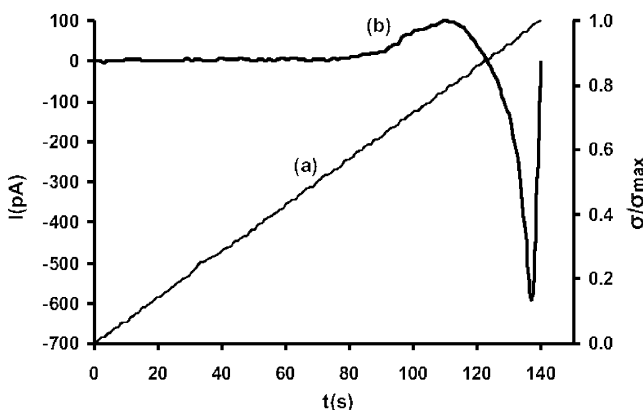


Fig. 4. Correlation of PSC and normalized stress with respect to time.

failure. It has to be noted that the same behaviour was recorded in all similar experiments that were carried out with all samples of the same matrix rock.

Finally, another set of experiments was conducted to investigate how samples from the same matrix rock react, in the case that they had already been damaged by previous deformation cycles. The sample was subjected to a constant stress rate of approximately 0.42 MPa/s, from zero stress and up to the stage before failure. PSC was recorded at stress values above  $\sim 0.6\sigma_{\max}$  (Fig. 5, curve a). Then, the stress was relieved and the sample was left to relax for 30 min. The above procedure was repeated twice at the same stress rate. During the second loading cycle, the measured PSC amplitude was smaller than that observed in the first cycle, as can be seen in Fig. 5 (curve b). During the third repetition of the experiment a very small PSC was recorded, as can be seen in Fig. 5 (curve c). On increasing the stress to the level of  $\sigma_{\max}$ , a large negative current-spike was recorded as in the previous set of experiments and failure occurred.

Although geomaterials are usually brittle, a repetitive stress-strain process may affect the elastic properties of the marble samples. Thus, the results of the above experiment may be explained in terms of the ‘‘work hardening’’ effect. When stress is applied to a ‘pristine’ rock sample and drives the material into the plastic deformation range, dislocations move and multiply and microcracks appear as described in Section 2. Then, an electric dipole field forming as per Eq. (1) may well be used to explanation of the form of the PSC shown in Fig. 5a. On applying stress for the second time, many of the existing dislocations are replaced by neighbouring partial dislocations as this process results in a reduction

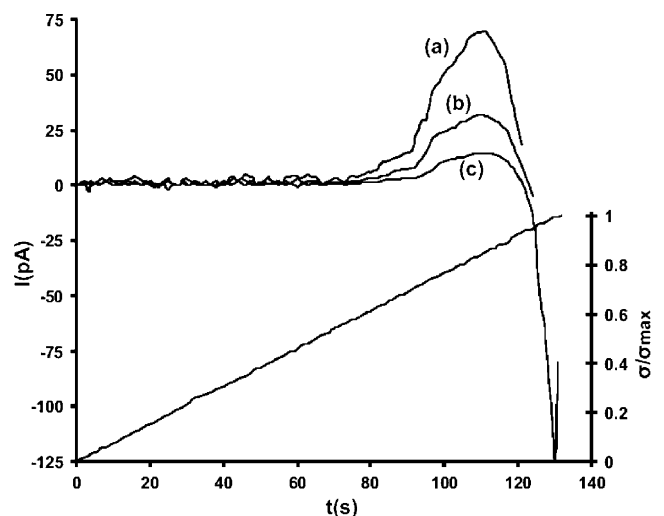


Fig. 5. Consecutive PSC curves at a constant stress rate indicative of the results of the ‘work hardening’ process. (a) Initial compression, (b) second compression, (c) final compression and up to fracture. On the right hand axis the normalized stress.

of the elastic energy of the sample (Feltham, 1966) This process does not necessarily result in an increase of the number of dipoles, thus, less charge is released to participate in the PSC and consequently a smaller current is generated, as also shown in Fig. 5b. Apparently, the sequence of stress-induced dislocations is physically limited only by the volume of the sample but the released charge being part of the total charge of the sample is a decreasing function of the number of stress-application repetitions. Fig. 5c appears to support this assertion.

#### 4. From the laboratory to the earthquake scale: expected source time functions and signal waveforms

The reported experiments have amply demonstrated that in dry rocks, microfracturing may produce macroscopic electric transients with intensity dependent on the mechanical state of the deforming material. The results are consistent with the predictions of the MCD/microfracturing model, with particular reference to the terminal stage of the process and prior to failure, when the material deforms plastically and non-linearly due to excessive accumulation of damage. A problem not answered (in fact not answerable by such experiments), is of whether these effects can scale up to the megascopic level of Earth (crustal) processes and generate observable EEP. On the other hand, it is very important to note that such a possibility is *not* contested by the experiments: if scaling up is possible, EEP signals are feasible, as shown by Tzanis and Vallianatos (2002). In this case, it should be possible to predict the form of this particular class of EEP phenomena (e.g. Tzanis et al., 2000; Tzanis and Vallianatos, 2002). Only essential elements of this theory will be presented here.

Brittle failure begins at the microscopic scale and cascades to the macroscopic by co-operative crack growth and coalescence in such a way, that fracturing at one scale (or level of the crack hierarchy) is part of damage accumulation at a larger scale. Once microfracturing begins, the number of propagating cracks (and the electric field) is first expected to rise sharply, but as the sustainable crack density is approached and stress/strain levels drop below a threshold value, it will decelerate and decline to zero when no more cracks can be produced. The duration of this process is unknown, but conceivably, it may require any time up to a few hours, depending on the size, mechanical and thermal state of the deforming volume.

The macroscopic behaviour of a large number of interacting cracks is, by nature, a problem of statistical mechanics and since cracks are organized in ensembles of distributed, interacting elements, it is appropriate to adopt a kinetic approach. A complete and comprehensive treatment of this problem has been given by

Czechowski (1991, 1995), who expands on assumptions similar to those of Boltzman's. The theory amounts to the kinetic equation

$$\begin{aligned} \frac{\partial f(\mathbf{x}, l, t)}{\partial t} + \frac{\partial [vpf(\mathbf{x}, l, t)]}{\partial l} \\ = \frac{1}{2} \int_0^l f(\mathbf{x}, l_1, t) f(\mathbf{x}, l - l_1, t) svp dl_1 \\ - f(\mathbf{x}, l, t) \int_0^\infty f(\mathbf{x}, l_1, t) svp dl_1 + N(l) \end{aligned} \quad (9)$$

where  $f(\mathbf{x}, l, t)$  is a size distribution function of cracks such that  $f(\mathbf{x}, l, t) \Delta \mathbf{x} \Delta l$  is the number of cracks which exist at time  $t$  within a volume element  $\Delta \mathbf{x}$  around a point  $\mathbf{x}$  and have sizes within  $\Delta l$  around size  $l$ , and where  $p$  and  $v$  are respectively the probability and velocity with which cracks may propagate. The LHS of Eq. (9) expresses the changes in the number of cracks as resulting from the interactions described by the RHS. Specifically, the first term in the RHS is the total number of 'gains', i.e. the number of binary interactions whereby cracks with (smaller) sizes  $l_1 < l$  collide and merge with cracks  $l < l_1$  to produce cracks with sizes  $l$ , where  $s = s(l, l_1, \bar{\sigma})$  is the cross-section of collisions,  $\bar{\sigma}$  is an average stress field and where the factor 1/2 prevents from counting an interaction twice. The second term in the RHS is the number of 'losses', i.e. the number of binary interactions whereby cracks of any size  $l_1$  forming a beam with flux density  $dI = vpf(\mathbf{x}, l_1, t) dl_1$  collide with crack  $l$  and consume it.  $N(l)$  is the nucleation term. The kinetic equation describes how cracks propagate and join each other with probability depending on the total cross-section of collisions between cracks. The quantities  $s$ ,  $v$ , and  $p$  may be functions of the size of cracks, stress field and properties of the rock. We are particularly interested in an analysis discretizing Eq. (9) in the size-space of cracks, according to

$$n_i(t) = \int_{L_{i-1}}^{L_i} f(l, t) dl,$$

so that the total number of cracks is divided into  $m$  populations  $n_i$ ,  $i = 1, 2, \dots, m$  with respect to their size.

Successive integrations of (9) over the intervals  $(0, L_1], (0, L_2], \dots, (L_M, \infty)$ , subject to the constraints  $0 = L_0 < L_1 < \dots < L_{M-1} < L_M = \infty$  and  $L_i - L_{i-1} = 1$  for  $i = 1, 2, \dots, M$ , produce a set of  $M$  coupled ordinary differential equations that describe the balance of gains and losses of any given group of cracks by mergence and by propagation. For instance,  $M = 3$  yields

$$\begin{aligned} \dot{n}_1 &= -(1 - 0.5k_1)n_1^2 - n_1n_2 - n_1n_3 + n_1 \\ \dot{n}_2 &= 0.5(k_2 - k_1)n_1^2 - (1 - 0.5k_2)n_2^2 - (1 - k_2)n_1n_2 \\ &\quad - n_2n_3 + n_2 \\ \dot{n}_3 &= 0.5(1 - k_2)(n_1^2 + 2n_1n_2 + n_2^2) - 0.5n_3^2 + n_3 \end{aligned} \quad (10)$$

where  $\dot{n}_i = (s_i v_i p_{i1})^{-1} \cdot (dn_i/dt)$ ,  $n_i n_j$  denotes the fusion of cracks  $n_i$  with cracks  $n_j$  and  $n_i = p_i (p_{i1} s_i)^{-1} \cdot [f(L_{i-1}, t) - f(L_i, t)]$  is the propagation term. The factors  $k_j$  determine the span of interactions between any two crack populations, with  $(1 - k_j)$  representing the extent of losses due to healing. For a decreasing  $f(l)$ ,  $0 < k_j < 1/2$ , with  $k_j = 1/2$  for  $f(l)$  constant.

The case  $M = 10$  has been developed by Czechowski (1995) and utilized by Tzanis et al. (2000) and Tzanis and Vallianatos (2002). Using the resulting 10 coupled ordinary differential equations and assuming a constant production rate for the smallest crack population, in Fig. 6a we present a simulation of how the corre-

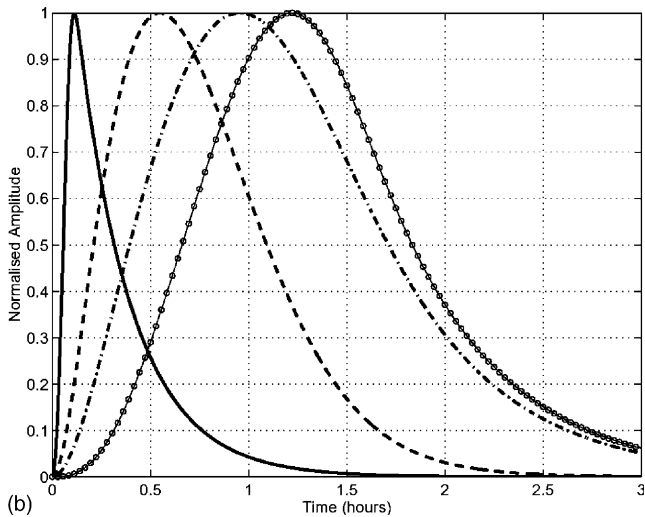
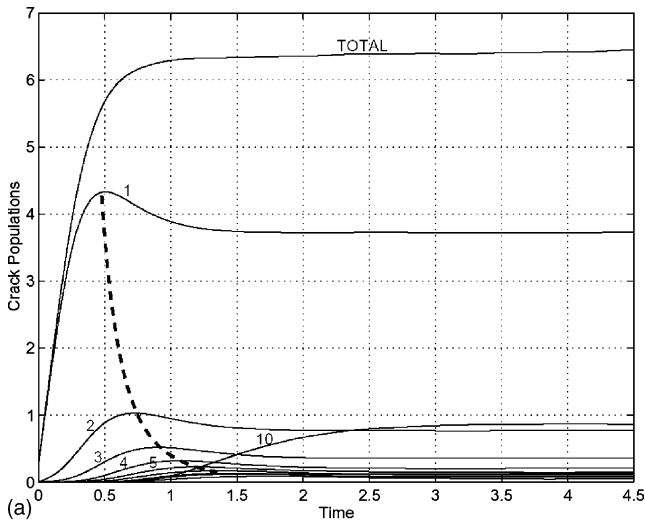


Fig. 6. (a) The evolution of 10 hierarchical crack populations following the kinetic theory of Czechowski (1995). A constant production rate for the smallest size crack population (No. 1) is assumed. The number of cracks are given in relative units. (b) Normalized time functions describing the evolution of the total number of cracks for different parameters of Eq. (11). Solid line,  $A = 0.3 \times 10^{-2}$ ,  $\beta = 2$ ,  $\alpha = -10^{-3}$ ; dashed,  $A = 0.2 \times 10^{-3}$ ,  $\beta = 2$ ,  $\alpha = -10^{-3}$ ; dash-dot,  $A = 0.2 \times 10^{-3}$ ,  $\beta = 2$ ,  $\alpha = 5 \times 10^{-4}$ ; open circles,  $A = 0.2 \times 10^{-3}$ ,  $\beta = 3$ ,  $\alpha = 5 \times 10^{-3}$ . In all cases  $\gamma = 1$ .

sponding 10 crack populations evolve, as well as the total number of cracks. The successive populations appear with a time delay following some power law (dashed line) such that the total number of cracks behaves like a step function, asymptotically converging to a constant value as the crack density approaches saturation. This can be approximated by

$$n(t) = N_0(1 - e^{-(at)^\gamma}) \quad (11)$$

Since only the active (propagating) cracks are electric field sources, their time function should be

$$\dot{n}(t) = N_0 \gamma a^\gamma t^{\gamma-1} e^{-(at)^\gamma} \quad (12)$$

where  $\alpha$  is a characteristic relaxation time and the exponent  $\gamma$  determines the shape. Note that (11) is in reality a Weibull cumulative distribution function and (12) the corresponding probability density function. Alternatively, an empirical description can be adopted, using a half step function such as is the error function (for  $t > 0$ ) for the rise time of the source, and assuming an exponential decay:

$$\dot{n}(t) = \text{erf}((At)^\beta) e^{-(at)^\gamma} u(t) \quad (13)$$

where  $u(t)$  is the Heaviside step function with  $u(t) = 1$  for  $t > 0$  and  $u(t) = 0$  for  $t \leq 0$ . The constant  $\beta$  determines the slope of the rise time and  $A$  is a characteristic time of the crack production processes, both dependent on material properties. Examples of (13) for different parameters  $A$ ,  $\alpha$  and  $\beta$  are shown in Fig. 6b; these are characteristic shapes expected from the related family of functions (12) and (13). Variations of crack counts with a bell shaped envelope have often been seen prior to rupture, in recent experiments involving large rock samples (Ponomarev et al., 1997; Feng and Seto, 1998, 1999; Baddari et al., 1999). Although much work is still needed to define the details, it appears that expressions (11)–(13) may comprise a phenomenological description of crack propagation processes over a wide spectrum of time scales.

It is quite apparent that by virtue of (1), the electric signal generated during microfracturing will be given by the convolution

$$\begin{aligned} \tilde{E}(\mathbf{r}, t) &= \dot{n}(t) * E(\mathbf{r}, t) \\ &= c_s \dot{n}(t) * \sum_{i=1}^N (\rho J)_i G(\mathbf{r}, \mathbf{r}_i) \cdot \left[ u(t) - u\left(t - \frac{l_i}{v_i}\right) \right] \end{aligned} \quad (14)$$

The duration of  $E(\mathbf{r}, t)$  is of the order of a few to several seconds when  $t_c \sim 10^{-7} - 10^{-4}$  s. Moreover, frequencies higher than a few Hz do not propagate to intermediate or large distances from the source (Vallianatos and Tzanis, 1998, 1999a). It is therefore expected that if  $\dot{n}(t)$  is much slower than  $E(\mathbf{r}, t)$ , its waveform will predominate and determine the waveform of the resulting EEP. If the source time function is sufficiently slow, only the

long periods of the resultant field  $\tilde{E}(\mathbf{r}, t)$  are allowed to propagate.

4.1. Two examples from the January 1983, M7 Kefallinia earthquake sequence (Ionian Sea)

One of the largest events to have occurred in the Ionian Sea region in the 20th century, this earthquake occurred offshore to the SW of Kefallinia island, Greece, on 12:41 GMT of 17 January 1983, at the coordinates 38.09° N, 20.19° E and a focal depth of 9 km (see Baker et al., 1997, for a review). Varotsos and Lazaridou (1991) claim to have recorded an electrical precursor to this earthquake at their PIR station, approximately 130 km SE of the epicentre, which they illustrate in Fig. 7 of their paper (see Fig. 7). We have reproduced a digital version of the longer periods of the signal by scanning their Fig. 7, enhancing the image and digitising it on a high resolution monitor. The digitized raw signal comprises a transient beginning on approximately 14:00 of 15 January 1983 and lasting for 1.5–2 hours, superimposed on a non-linear variation of the background (Fig. 8). On removing the background, we obtain a very strong E–W component (25 mV over 50 m), but very weak N–S (Fig. 8 bottom). The E–W waveform has an asymmetric bell shape, with faster rise time and a slower exponential type decay; for most of its duration, it stands clearly above noise, the peak amplitude of which is approximately 20% of the peak signal amplitude. The later times of the signal, however, are obscured, and there is no real way of telling the exact duration of the decay phase. The long period E–W components can be easily fitted with functions of the form (12) and (13). Recall that both functions are phenomenological descriptions of the signal shape only, since we cannot as yet estimate the amplitude. Therefore, we may only attempt to fit the signal and the model normalized with respect to their maximum values. In Fig. 9 we present

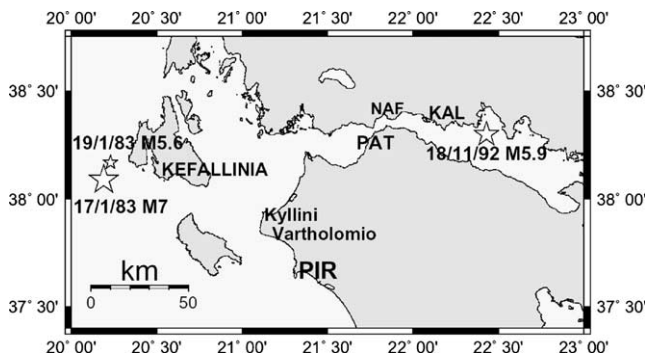


Fig. 7. The stars show the epicentres of the 17-1-83 M7 Kefallinia, the 19-1-83 M5.6 Kefallinia and the 18-11-1992 M5.9 Galaxidi events. PIR is the location where the ‘precursory’ signals from the Kefallinia events were detected; PAT is the observation location for the Galaxidi event.

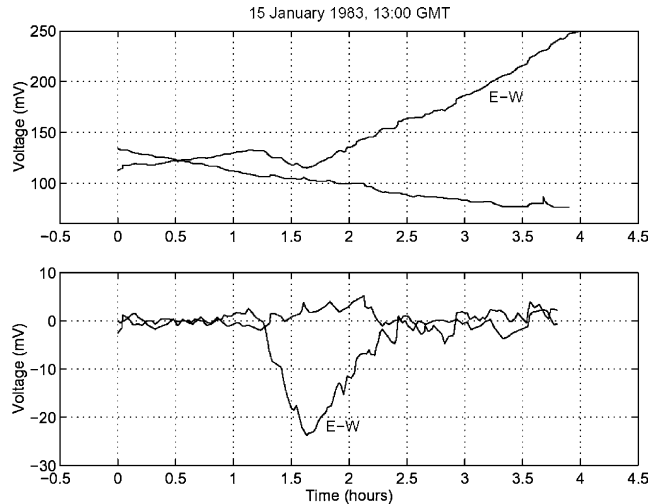


Fig. 8. The upper panel shows the digitized signal recorded on 14:00 GMT of 15 January 1983 at Pyrgos, Greece (PIR), and reported by Varotsos and Alexopoulos (1984) as a precursor to the 17 January 1983 Kefallinia earthquake ( $\Delta \approx 130$  km). The lower panel shows the transient signal after removing the background. Hour 0 in the time axis corresponds to 13:00 GMT.

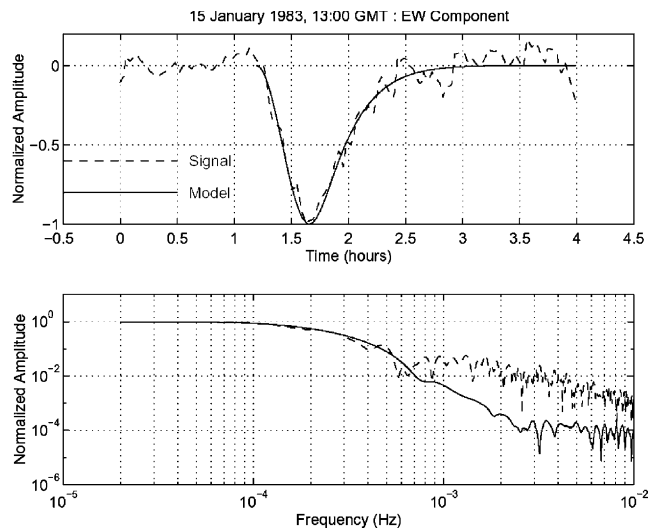


Fig. 9. A model of the normalized long period E–W component of the 15-1-83 signal (Fig. 10) in the time domain (top) and frequency domain (bottom).

a model based on Eq. (13), with  $\gamma = 1$  (fixed),  $A \approx 5.3 \times 10^{-4} \text{ s}^{-1}$ ,  $\beta \approx 2.1$  and  $\alpha \approx 9.9 \times 10^{-4} \text{ s}^{-1}$  ( $2\pi/\alpha \approx 6300 \text{ s}$  is approximately the duration of the model and  $1/\alpha$  is a characteristic relaxation time).

A large  $M = 5.6$  aftershock of this event occurred on 00:02 GMT of 19 January 1983, at 38.11° N and 20.25° E (Fig. 7). Varotsos and Lazaridou (1991) again claim to have recorded a precursor at PIR, which they illustrate in Fig. 8 of their paper. This signal was also reproduced digitally. The EW component is shown in Fig. 10a and b

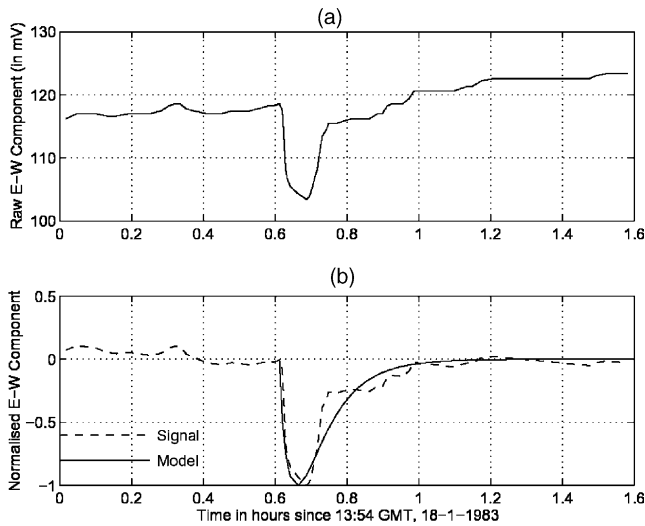


Fig. 10. (a) The digitized E–W component of a transient signal recorded on 14:30 GMT of 18 January 1983 at Pyrgos, Greece (PIR), and reported by Varotsos and Alexopoulos (1984) as a precursor to the M5.6, 19 January 1983 aftershock of the Kefallinia main shock ( $A \approx 130$  km). (b) A model (solid line) of the signal (broken line) after removing a linear trend. Hour 0 in the time axis roughly corresponds to 13:54 GMT.

(broken line, after removing a linear trend). Again, it comprises an asymmetric-bell shaped variation with very fast rise time and a slower exponential decay, beginning on approximately 14:30 GMT of 18 January 1983 and lasting for almost 50 min. The solid line in Fig. 10b is a model based on Eq. (13), with  $\gamma = 1$ ,  $A \approx \alpha 3.15 \times 10^{-3} \text{ s}^{-1}$ , and  $\beta \approx 0.74$ ; here as well  $2\pi/\omega \approx 1990$  s (55 min) is approximately the duration of the signal and model.

It is important to note that both these signals belong to the small ensemble of transients used by Varotsos and Lazaridou (1991) to construct their amplitude–magnitude empirical scaling law, of the form  $\log(\Delta V) = cM + d$ , with  $c = 0.3\text{--}0.4$  a universal value. A number of authors have independently argued, or shown, that this law derives from the fundamental fractal scaling of the electric field sources (Sornette and Sornette, 1990; Molchanov, 1999; Vallianatos and Tzani, 1999b). Such properties are not likely to have been generated by anthropogenic noise and indicate that both signals may be a real, long range EEP.

#### 4.2. A possible EEP to the 18 November 1992, M5.9 Galaxidi Earthquake (Gulf of Corinth, Central Greece)

The event with  $M_S = 5.9$  occurred offshore at  $38.30^\circ$  N,  $22.43^\circ$  E (ISC) with a focal depth of 7–10 km. In hindsight, we can recognize several phenomena that may be interpreted as precursory to this earthquake. According to Ifantis et al. (1993), a large number of very

small earthquakes ( $M < 2$ ), were recorded at the station NAF of the local permanent network of the University of Patras (PAT Fig. 7), on 11–11–1992. These events reached a peak rate of several hundreds per day. We did not find any other published account of this phenomenon. Abbad (1993) reports a strong radon emission anomaly, which started building up by the late hours of 12 November at station KAL (Fig. 7), approximately 20 km to the NW of the epicentre and culminated the next day. These observations are *direct* evidence of microfracturing, given that radon is released from the host rock by such a process.

A transient electric variation was observed on 12 November 1992, at the University of Patras Campus, approximately 70 km west of the epicentre (Fig. 11). Ifantis et al. (1993) report this signal as EEP (1996, in *their* Fig. 10), but do not make any attempt to identify and authenticate it, appearing content with the fact that “no other anomaly of the geoelectric field was recorded prior to the event”. The published signal was sufficiently clear and annotated, as to warrant digital reproduction. It comprises two distinct waveforms with identical polarization. The first arrived just after 11:20 GMT. It had peak-to-peak amplitude 12.3 mV, lasted for a little more than one hour and resembled a damped sinusoid (Fig. 11a). The second arrived just after 12:40 GMT, had a peak amplitude of 9.5 mV, lasted for almost 1 h and had an asymmetric bell shape (Fig. 11c). In spite of the different waveforms, the identical polarization of the two signals points toward common or at least proximate source regions.

The first signal cannot be modelled exactly with Eqs. (12) or (13). In keeping the discussion simple, we introduce the function

$$\dot{n}(t) = t^\beta \cdot \sin(\xi t) \cdot e^{-\alpha t} u(t) \quad (15)$$

describing a linear system with feedback proportional to the derivative of its output (see Rohrs et al., 1993). Such a system could possibly describe crack propagation, if stress is the input depending on a set of past state variables, and strain rate the output. This system would be self-regulating, with its state continuously varying with time. It may be that Eq. (15) represents a more general case, with Eqs. (12) and (13) being time functions of simpler (and possibly more common) processes without this type of feedback. This hypothesis cannot be tested because we know only this example and we do not know under which conditions the system (15) would be realizable. The signal may be fitted with the parameters  $\alpha = 0.001772$ ,  $\beta = 1.25$ ,  $\xi = 0.001728$  and the model is shown in Fig. 11b. Note that the sinusoidal modulator frequency ( $\xi$ ) is comparable to the characteristic time ( $\alpha$ ) of the signal, indicating the time constant of the hypothesized feedback mechanism. The second signal may be better modelled with Eq. (13) as shown in Fig. 11d.

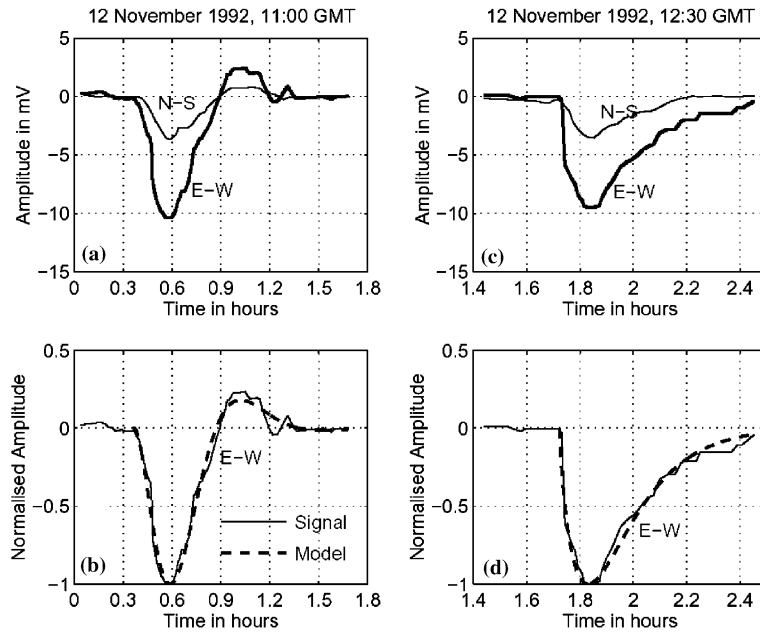


Fig. 11. (a) The first signal recorded by Ifantis et al. (1993) on 11:20 GMT of 12/11/1992 at Patras, Greece, and reported as precursor to the 18/11/1992 Galaxidi earthquake. Hour 0 corresponds to 11:00 GMT. (b) A model of the normalized long period E-W component constructed with Eq. (15). (c) The second signal of Ifantis et al. (1993), with arrival at 12:40 GMT of 12/11/1992. The time axis is annotated relative to that of (a). (d) A model of the normalized E-W component constructed with Eq. (13).

## 5. Concluding remarks

The spontaneous generation of transient electric current during fracturing of non-piezoelectric rock samples has long been observed by experiment, but the underlying mechanism(s) have not been clarified. The work presented herein was essentially an attempt to understand the physics of the electrification processes in dry (resistive) rock samples, focusing on the hypothesis that the main source of this current may be the motion of charged edge dislocations (MCD) during crack formation and propagation, which is expected at the terminal phase of the deformation cycle. In particular, we targeted properties relating to the dependence of the current on the mechanical state of the deforming material (damage accumulation and stress and strain rates).

The experiments confirmed the generation of pressure-stimulated currents (PSC) as expected by the MCD model. The PSC was linearly related to the stress rate ( $d\sigma/dt$ ), so long as the stressed material deformed elastically. Deviation from linearity arose when the applied stress drove the specimen into the plastic deformation range; this effect has been attributed to the dependence of the PSC on the stress rate and, ultimately, to the inverse of the changing (decreasing) Young's modulus. The emitted current appears very intense and non-linear just prior to failure, where massive crack propagation implies massive MCD processes. Repeated cycles of deformation are associated with progressively weaker

current emission, indicating the strong dependence of electrification on the residual damage, i.e. the residual number of unhealed cracks, which should correspondingly increase (existing cracks that do not open should not generate current). Overall, the results are consistent with, and render support to the concept of electrification by MCD/microfracturing. Other mechanisms are not excluded of course, but are rather considered to accompany and supplement the drastic MCD process.

Whether these process can scale up to earthquake-size volumes and produce an observable precursor is another question. If the laboratory results are an indicator, then this possibility cannot be ruled out. The source of the precursor might be the motion of charged edge dislocations during massive crack formation and propagation, which in the case of earthquakes is expected to be a short-lived process at the terminal phase of the cycle. The observable macroscopic ULF field would be generated by the superposition of multiple simultaneous tiny sources (individual cracks). From a theoretical point of view, it is readily demonstrable that such a process is feasible and efficient. It is also possible to model the evolution of large crack ensembles and derive the expected time functions of transient EEP events: the result is a family of asymmetric-bell shaped time functions that may appear isolated or in groups. The model has been successfully applied to the analysis of field observations taken from the literature.

The model makes specific predictions about the properties of a certain class of transient electric

precursors, but while it is plausible and testable, it is still far from being complete and verified. It is clear that a great deal of work is needed before one can claim a working theory of the earthquake preparation process, but it is also apparent that observed signals can indeed be interpreted in terms of real and testable physics and their associated generic theories of the source.

## References

- Abbad, S., 1993. Etude des variations de l'activité volumique radon en fonction des paramètres météorologiques et géologiques. Doctoral Dissertation, University of Paris VII (in French).
- Baddari, K., Sobolev, G.A., Frolov, A., Ponomarev, A., 1999. An integrated study of physical precursors of failure in relation to earthquake prediction, using large scale rock blocks. *Anna. Geof.* 42, 771–787.
- Baker, C., Hatzfeld, D., Lyon-Caen, H., Papadimitriou, E., Rigo, A., 1997. Earthquake mechanisms of the Adriatic sea and western Greece: implications for the oceanic subduction–continental collision transition. *Geophys. J. Int.* 131, 559–594.
- Bernard, P., 1992. Plausibility of long distance electrotelluric precursors to earthquakes. *J. Geophys. Res.* 97, 17531–17546.
- Bernard, P., Le Mouél, J.L., 1996. On electrotelluric signals. In: Lighthill, J. (Ed.), *A Critical Review of VAN*. World Scientific, Singapore, pp. 118–152.
- Czechowski, Z., 1991. A kinetic model of crack fusion. *Geophys. J. Int.* 104, 419–422.
- Czechowski, Z., 1995. Dynamics of fracturing and cracks. In: Teisseyre, R. (Ed.), *Theory of Earthquake Premonitory and Fracture Processes*. Polish Scientific Publishers, pp. 447–469.
- Chen, D.-Y., Zhang, D.-H., Sun, Z.-J., 1994. ULF electric-potential changes prior to the fracture in rock samples. In: Hayakawa, M., Fujinawa, Y. (Eds.), *Electromagnetic Phenomena Related to Earthquake Prediction*. Terra Scientific Publishing Co., pp. 323–329.
- Dobrovolsky, I.P., Gershenzon, N.I., Gokhberg, M.B., 1989. Theory of electrokinetic effects occurring at the final stage in the preparation of a tectonic earthquake. *Phys. Earth Planet. Inter.* 57, 144–156.
- Enomoto, Y., 1996. Notes on generation and propagation of seismic transient electric signals. In: Lighthill, J. (Ed.), *A Critical Review of VAN*. World Scientific, Singapore, pp. 324–331.
- Enomoto, J., Hashimoto, H., 1990. Emission of charged particles from indentation fracture of rocks. *Nature* 346, 641–643.
- Enomoto, Y., Shimamoto, T., Tsutsumi, A., Hashimoto, H., 1994. Transient electric signals prior to rock fracturing: potential use as an immediate earthquake precursor. In: Hayakawa, M., Fujinawa, Y. (Eds.), *Electromagnetic Phenomena Related to Earthquake Prediction*. Terra Scientific Publishing Co., Tokyo, pp. 253–259.
- Ernst, T., Jankowski, J., Rozluski, C., Teisseyre, R., 1993. Analysis of the electromagnetic field recorded in the Friuli seismic zone, NE Italy. *Tectonophysics* 224 (1), 141–148.
- Feltham, P., 1966. *Deformation and Strength of Materials*. Butterworths.
- Feng, X.-T., Seto, M., 1998. Neural network dynamic modelling of rock microfracturing sequences under triaxial compressive stress conditions. *Tectonophysics* 292, 293–309.
- Feng, X.-T., Seto, M., 1999. Fractal structure of the time distribution of microfracturing in rocks. *Geophys. J. Int.* 136, 275–285.
- Fenoglio, M.A., Johnston, M.J.S., Byerlee, J., 1995. Magnetic and electric fields associated with changes in high pore pressure in fault zones—Application to the Loma Prieta ULF emissions. *J. Geophys. Res.* 100 (B7), 12951–12958.
- Fiffolt, D.A., Petrenko, V.F., Schulson, E.M., 1993. Preliminary study of electromagnetic emissions from cracks in ice. *Philos. Mag.* B 67, 289–299.
- Freund, F., 2000. Time-resolved study of charge generation and propagation in igneous rocks. *J. Geophys. Res.* B 105, 11001–11019.
- Freund, F., Borucki, J.G., 1999. Charge carrier generation and charge cloud propagation following 100 m/sec impacts on igneous rocks. In: Hayakawa, M. (Ed.), *Atmospheric and Ionospheric Electromagnetic Phenomena Associated with Earthquakes*. Terra Scientific Publishing Co., Tokyo, pp. 839–857.
- Gensane, O., Konyukov, B., Le Mouél, J.-L., Morat, P., 1999. SP coseismic signals observed on an electrodes array in an underground quarry. *Geophys. Res. Lett.* 26 (23), 3529–3532.
- Gokhberg, M.B., Gufeld, I.L., Gershenzon, N.I., Pilipenko, V.A., 1985. Electromagnetic effects during rupture of the Earth's crust. *Izvestiya. Earth Phys.* 21 (1), 52–63.
- Hadjicontis, V., Mavromatou, C., 1994. Transient electric signals prior to rock failure under uniaxial compression. *Geophys. Res. Lett.* 21, 1687–1690.
- Hadjicontis, V., Mavromatou, C., 1996. Laboratory investigation of electric signals preceding earthquakes. In: Lighthill, J. (Ed.), *A Critical Review of VAN*. World Scientific, Singapore, pp. 105–117.
- Hallbauer, D.K., Wagner, H., Cook, N.G.W., 1973. Some observations concerning the microscopic and mechanical behaviour of quartzite specimens in stiff, triaxial compression tests. *Int. J. Rock Mech. Min. Sci. Geomech. Abstr.* 10, 713–726.
- Hayakawa, M. (Ed.), 1999. *Atmospheric and Ionospheric Electromagnetic Phenomena Associated with Earthquakes*. Terra Scientific Publishing Co., Tokyo.
- Hayakawa, M., Molchanov, O. (Eds.), 2002. *Seismoelectromagnetics (Lithosphere–Atmosphere–Ionosphere Coupling)*. Terra Scientific Publishing Co., Tokyo, p. 2002.
- Hayakawa, M., Fujinawa, Y. (Eds.), 1994. *Electromagnetic Phenomena Related to Earthquake Prediction*. Terra Scientific Publishing Co., Tokyo.
- Ifantis, A., Tselentis, G.-A., Varotsos, P., Thanassoulas, C., 1993. Long term variations of the Earth's electric field preceding two earthquakes in Greece. *Acta Geophys. Polonica*, XLI 4, 337–350.
- Johnston, M.J.S., 1997. Review of electrical and magnetic fields accompanying seismic and volcanic activity. *Surv. Geophys.* 18, 441–475.
- Jouniaux, L., Pozzi, J.-P., 1995a. Permeability dependence of streaming potential in rocks for various fluid conductivities. *Geophys. Res. Lett.* 22 (4), 485–488.
- Jouniaux, L., Pozzi, J.-P., 1995b. Streaming potential and permeability of saturated sandstones under triaxial stress: Consequences for electrotelluric anomalies prior to earthquakes. *J. Geophys. Res.* 100 (B6), 10197–10209.
- Jouniaux, L., Pozzi, J.-P., 1997. Laboratory measurements of anomalous 0.1–0.5 Hz streaming potential under geochemical changes: Implications for electrotelluric precursors to earthquakes. *J. Geophys. Res.* 102 (B7), 15335–15343.
- Kleftakis, S., Agioutantis, Z., Stiakakis, C., 2000. Numerical Simulation of the uniaxial compression test including the specimen–platen interaction. *Computational methods for shell and spatial structures*, IASS-IACM.
- Lei, X.L., Kusunose, K., Nishizawa, O., Cho, A., Satoh, T., 2000. On the spatiotemporal distribution of acoustic emissions in two granitic rocks under triaxial compression: the role of pre-existing cracks. *Geophys. Res. Lett.* 27, 1997–2000.
- Mizutani, H., Ishido, T., Yokokura, T., Ohnishi, S., 1976. Electrokinetic phenomena associated with earthquakes. *Geophys. Res. Lett.* 3, 365–368.
- Molchanov, O.V., 1999. Fracturing as underlying mechanism of seismo-electric signals. In: Hayakawa, M. (Ed.), *Atmospheric and Ionospheric Electromagnetic Phenomena Associated with Earthquakes*. Terra Scientific Publishing Co., Tokyo, pp. 349–356.

- Molchanov, O.V., Hayakawa, M., 1998. On the generation mechanism of ULF seismogenic electromagnetic emissions. *Phys. Earth Planet. Int.* 105, 201–210.
- Morgan, F.D., Williams, E.R., Madden, T.R., 1989. Streaming potential properties of Westerly granite with applications. *J. Geophys. Res.* 94, 12449–12461.
- Nitsan, U., 1977. Electromagnetic emission accompanying fracture of quartz-bearing rocks. *Geophys. Res. Lett.* 4, 333–337.
- Ogawa, T., Oike, K., Miura, T., 1985. Electromagnetic radiation from rocks. *J. Geophys. Res.* 90, 6245–6249.
- Park, S.K., Johnston, M.J.S., Madden, T.R., Morgan, F.D., Morison, H.F., 1993. Electromagnetic precursors to earthquakes in the ULF band: A review of observations and mechanisms. *Rev. Geophys.* 31 (2), 117–132.
- Patella, D., Tramacere, A., Di Maio, R., 1997. Modelling earth current precursors in earthquake prediction. *Anna. Geof.* XL (2), 495–517.
- Ponomarev, A.V., Zavyalov, A.D., Smirnov, V.B., Lockner, D.A., 1997. Physical modelling of the formation and evolution of seismically active fault zones. *Tectonophysics* 277, 57–81.
- Rohrs, C.E., Melsa, J.L., Schultz, D.G., 1993. *Linear Control Systems*. McGraw-Hill, New York.
- Sasaoka, H., Yamanaka, C., Ikeya, M., 1998. Measurements of electric potential variation by piezoelectricity in granite. *Geophys. Res. Lett.* 25 (12), 2225–2228.
- Scholz, C.H., Sykes, L.R., Aggarwal, Y.P., 1973. Earthquake prediction: A physical basis. *Science* 181, 803–809.
- Scudiero, L., Dickinson, J.T., Enomoto, Y., 1998. The electrification of flowing gases by mechanical abrasion of mineral surface. *Phys. Chem. Minerals* 25, 566–573.
- Slifkin, L., 1993. Seismic electric signals from displacement of charged dislocations. *Tectonophysics* 224, 149–152.
- Sornette, A., Sornette, D., 1990. Earthquake rupture as a critical point: consequences for telluric precursors. *Tectonophysics* 179, 327–334.
- Stavarakas, I., Anastasiadis, C., Triantis, D., Vallianatos, F., 2003. Piezo stimulated currents in marble samples: precursory and concurrent-with-failure signals. *Natural Hazards Earth Syst. Sci.* 3, 243–247.
- Surkov, V., 1999. ULF electromagnetic perturbations resulting from the fracture and dilatancy in the earthquake preparation zone. In: Hayakawa, M. (Ed.), *Atmospheric and Ionospheric Electromagnetic Phenomena Associated with Earthquakes*. Terra Scientific Publishing Co., Tokyo, pp. 371–382.
- Tomizawa, I., Hayakawa, M., Yoshino, T., Ohta, K., Okada, T., Sakai, H., 1994. Observation of ELF/VLF electromagnetic variations associated with a seismic experimental explosion. In: Hayakawa, M., Fujinawa, Y. (Eds.), *Electromagnetic Phenomena Related to Earthquake Prediction*. Terra Scientific Publishing Co., Tokyo, pp. 337–347.
- Tuck, B.T., Stacey, F.D., Starkey, J., 1977. A search for the piezoelectric effect in quartz-bearing rock. *Tectonophysics* 39, 7–11.
- Tzani, A., Vallianatos, F., 2001. A critical review of electric earthquake precursors. *Anna. Geof.* 44 (2), 429–460.
- Tzani, A., Vallianatos, F., 2002. A physical model of electrical earthquake precursors due to crack propagation and the motion of charged edge dislocations. In: Hayakawa, M., Molchanov, O.A. (Eds.), *Seismo Electromagnetics: Lithosphere–Atmosphere–Ionosphere Coupling*. TERRAPUB, Tokyo, pp. 117–130.
- Tzani, A., Vallianatos, F., Gruszow, S., 2000. Identification and discrimination of transient electrical earthquake precursors: fact, fiction and some possibilities. *Phys. Earth Planet. Int.* 121, 223–248.
- Turcotte, D.L., Newman, W.I., Shcherbakov, R., 2003. Micro and macroscopic models of rock fracture. *Geophys. J. Int.* 152, 718–728.
- Vallianatos, F., Tzani, A., 1998. Electric current generation associated with the deformation rate of a solid: preseismic and coseismic signals. *Phys. Chem. Earth* 23, 933–938.
- Vallianatos, F., Tzani, A., 1999a. A model for the generation of precursory electric and magnetic fields associated with the deformation rate of the earthquake focus. In: Hayakawa, M. (Ed.), *Atmospheric and Ionospheric Electromagnetic Phenomena Associated with Earthquakes*. Terra Scientific Publishing Co., Tokyo, pp. 287–305.
- Vallianatos, F., Tzani, A., 1999b. On possible scaling laws between electric earthquake precursors (EEP) and earthquake magnitude. *Geophys. Res. Lett.* 26 (13), 2013–2016.
- Vallianatos, F., Tzani, A., 2003. On the nature, scaling and spectral properties of pre-seismic ULF signals. *Natural Hazards Earth Syst. Sci.* 3, 237–242.
- Varotsos, P., Alexopoulos, K., 1984. Physical properties of the variations of the electric field of the Earth preceding earthquakes, I. *Tectonophysics* 110, 73–98.
- Varotsos, P., Lazaridou, M., 1991. Latest aspects of earthquake prediction in Greece, based on seismic electric signals. *Tectonophysics* 188, 321–347.
- Varotsos, P., Alexopoulos, K., Lazaridou, M., 1993. Latest aspects on earthquake prediction in Greece based on seismic electric signals II. *Tectonophysics* 224, 1–37.
- Warwick, J.W., Stoker, C., Meyer, T.R., 1982. Radio emission associated with rock fracture: possible application to the great Chilean earthquake of May 22, 1960. *J. Geophys. Res.* 87, 2851–2859.
- Whitworth, R.W., 1975. Charged dislocations in ionic crystals. *Adv. Phys.* 24, 203–304.
- Yoshida, S., Manjgaladze, P., Zilpimiani, D., Ohnaka, M., Nakatani, M., 1994. Electromagnetic emissions associated with frictional sliding of rock. In: Hayakawa, M., Fujinawa, Y. (Eds.), *Electromagnetic Phenomena Related to Earthquake Prediction*. Terra Scientific Publishing Co., Tokyo, pp. 307–322.
- Yoshida, S., Uyeshima, M., Nakatani, M., 1997. Electric potential changes associated with a slip failure of granite: Preseismic and coseismic signals. *J. Geophys. Res.* 102, 14883–14897.
- Yoshida, S., Oswald, C.C., Sammonds, P.R., 1998. Electric potential changes prior to shear fracture in dry and saturated rocks. *Geophys. Res. Lett.* 25 (10), 1557–1580.